Self-Assembly and Molecular Dynamics of Copolymers of γ-Methyl-L-glutamate and Stearyl-L-glutamate

A. Gitsas and G. Floudas*

Department of Physics, University of Ioannina, P.O. Box 1186, 451 10 Ioannina, Greece, and Foundation for Research and Technology-Hellas (FORTH), Biomedical Research Institute (BRI)

M. Dietz, M. Mondeshki, H. W. Spiess, and G. Wegner

Max-Planck-Institut für Polymerforschung, D-55021 Mainz, Germany

Received April 3, 2007; Revised Manuscript Received September 7, 2007

ABSTRACT: We report on the self-assembly and molecular dynamics in a series of poly(γ-methyl-L-glutamate-*co*-γ-stearyl-L-glutamate) [poly(MLG-*co*-SLG)] using thermodynamic (differential scanning calorimetry), structural (wide-angle X-ray scattering and ^{13}C solid-state NMR), as well as dynamic (dielectric spectroscopy and site-specific solid-state NMR) techniques. Stearyl crystallization takes place in the copolymers with $w_{PSLG} \geq 18\%$ which reflects changes of the hydrocarbon side chains conformation. Extruded fibers of the copolymers are composed of both α-helical and β-sheet secondary structures oriented along the fiber axis with a bottleneck structure with MLG/SLG sequences forming the neck and more distant SLG sequences forming the bottle. This supramolecular organization has direct consequences on the dynamics. Two dielectrically active processes with strong temperature dependences were found. Site-specific NMR allowed the identification of the geometry of motions. One is associated with small-amplitude motions of amorphous segments along the polypeptide backbone and at the chain ends that freeze at the liquid-to-glass transition. The slower process is associated with the relaxation of the α-helical peptide secondary structure. The analysis of the dielectric strength associated with the slower process revealed that helices are objects of low persistence.

I. Introduction

Recent studies on "shape-persistent" macromolecules such as "hairy rod" polymers,[1] composites made of stiff macromolecules with flexible side groups, and α-helical synthetic polypeptides revealed some intriguing dynamic features.[2] For example, both systems, similar to amorphous polymers or glass-forming liquids in general, exhibit a dynamic process (α-process) that freezes at the liquid-to-glass temperature (T_g) and have at least one Arrhenius process in the glassy state. To understand the origin of this dynamic behavior, we have studied the dynamics in model "hairy rod" polymers composed of poly(*p*-phenylene) backbones substituted with either short ethylene oxide side groups[3] or with sulfonate ester and dodecyl side groups[4] as well as several synthetic polypeptides.[5,6] In the former system,[3] the combination of dielectric spectroscopy (DS) with various NMR techniques allowed the complete assignment of the dynamic processes associated with the two relaxations. It turned out that different molecular mobilities contribute to the α-process, including the relaxation of "fast" outer ethylene oxide units, small-angle fluctuations of the substituted rings, and the unfreezing of internal backbone modes. The β-process, on the other hand, was assigned to a very localized motion of the ethylene oxide side groups.

Similarly, the origin of the α-process in α-helical polypeptides has been recently[5,6] explored by combining temperature- and pressure-dependent dielectric spectroscopy (DS) techniques. Again, intramolecular dynamics of amorphous backbone segments were found to be responsible for the freezing of the dynamics at the respective T_g.

Other studies on the conformation, molecular dynamics, and spatial heterogeneities of stiff macromolecules bearing flexible side chains by means of X-ray scattering and site-specific NMR techniques suggested a layered structure of the rodlike polymer backbone with phase separated hydrocarbon side chains.[7−9] In addition, the side chains were found to form crystalline as well as amorphous domains depending on the nature of the main polymer chains and their organization.[8] The interlayer separation between the main chains, formed by para-substituted aromatic units linked by ester, amide, or imide groups, was interpreted in terms of different conformations and mobilities of the hydrocarbon chains. Moreover, in copolymers of residues with different side chain lengths, the layer distance changed to ensure space filling packing of the side chains.[9]

Poly(γ-*n*-alkyl L-glutamates) (PnALG) combine the "hairy rod" structure with the polypeptide backbone and can be considered as model systems in studying the interplay between molecular mobility and supramolecular organization. Systematic investigations of PnALGs as a function of the alkyl length, *n*, revealed flexible side groups for $n < 10$, whereas for $n \geq 10$, the side groups could crystallize giving rise to paraffin-like crystallites.[10−12] However, in many of these earlier studies a perfectly α-helical secondary peptide structure was assumed rather than found experimentally. In addition to the homopolymers, the molecular dynamics of the side groups in poly(γ-methyl-L-glutamate-*co*-γ-stearyl-L-glutamate) [poly(MLG-*co*-SLG)] copolymers with stearyl compositions in the range from 0 to 83% were investigated[13] by electron spin resonance using a spin-probe technique and ^{13}C cross-polarization magic-angle spinning (^{13}C CP-MAS) NMR. From the C_α and amide C═O chemical shifts, it was concluded that all copolymers take on the α-helical conformation independent of stearyl content. It was further assumed that the helices are perfectly rigid. On the basis of this assumption, the side group region in the copolymers at temperatures below the melting point (T_m') was divided into

* Corresponding author. E-mail: gfloudas@cc.uoi.gr.

10.1021/ma070792i CCC: $37.00
Published on Web 10/20/2007

three "phases" composed of semiflexible side groups of MLG and inner SLG side groups attached to the rigid α-helical backbones, amorphous stearyl groups and of crystalline stearyl groups.

An earlier dynamic investigation[14] on a single poly(MLG-*co*-SLG) with 30% stearyl content (MS30, below we use the abbreviation MS*x* where *x* stands for the percentage of stearyl groups) with various NMR techniques and with dielectric spectroscopy (DS) revealed a hierarchy of mobilities, from a local motion (γ-process) of the carboxyl side group dipole with an Arrhenius temperature dependence and an activation energy of ~43 kJ/mol to the β-process attributed to the dynamic glass transition of amorphous ester side group dipoles, to the α-process, discussed in terms of a restricted motion (libration) or chopstick motion of a rodlike α-helix. The rod dynamics in the same copolymer were determined by measuring the interfacial width between protonated and deuterated stacks.[15] In the latter study, the absence of the center of mass diffusion of rods between the protonated and deuterated layers was discussed in terms of the high viscosity of the side chains forming the matrix or densely packed rods.

Copolymers of MLG and SLG are model systems of molecular reinforced liquids or nanocomposites; the side chains form the liquid matrix and the embedded rods are reinforcing elements that provide the required mechanical stability. In addition, optical and thermal investigations revealed low losses and high thermal stability, respectively, in Langmuir−Blodgett (LB) films of poly(MLG-*co*-SLG). Understanding the self-assembly and the associated dynamics is essential in the design of LB films and devices based on such supramolecular architectures. Nevertheless, the detailed self-assembly and the dynamics have not been explored as of yet. In the present work we explore the interplay between supramolecular organization and the molecular dynamics in a series of poly(MLG-*co*-SLG) covering a greater composition range aiming at providing a realistic structural picture. For this purpose we study the thermodynamic transitions with differential scanning calorimetry (DSC), the peptide secondary structure (α-helices/β-sheets), and side chain conformation (gauche/trans) with ^{13}C cross-polarization (CP) solid-state NMR and wide-angle X-ray scattering (WAXS), and the dynamics with dielectric spectroscopy and site-specific solid-state NMR techniques.[16] DS and site-specific NMR methods provide, respectively, the time scales and geometry of motions. We found a "dynamic" structure composed of polypeptide α-helices/β-sheets with a bottleneck structure with amorphous MLG units forming the neck and more distant SLG units forming the bottle and explored the consequences of self-assembly on the dynamics.

II. Experimental Part

Synthesis. All chemicals were purchased from Sigma-Aldrich and were used without further purification unless otherwise stated. The polymers listed in Table 1 were synthesized by polymerization of the corresponding amino acid *N*-carboxyanhydride (NCA) as described below (Schemes 1 and 2). Hexyl amine was dried over CaH_2 and was freshly distilled prior to use in polymerization. All reactions were performed under argon and were monitored by thin-layer chromatography (TLC) using a methanol/chloroform (4:1) eluent system and ninhydrin as a staining agent for TLC. γ-Octadecyl-L-glutamate (**II**) was prepared following the procedure described by Wassermann et al.[17]

General Procedure for Synthesis of NCAs. A procedure similar to one described in the literature was used for the synthesis of the desired NCA monomers.[18] Rather than using the toxic phosgene gas, here, a 40% excess of trichloromethyl chloroformate (diphosgene) in dry THF was used to react with the amino acid. Activated charcoal acts as a catalyst in the decomposition process of diphosgene. The reaction proceeds for an hour at 55 °C before the charcoal is removed by filtration through celite powder placed on a glass filter. The filtrate is reduced, and the residual oil crystallizes upon addition of hexane. The NCA monomers were purified three times by reprecipitation in ethyl acetate/hexane (1:4).

Table 1. Molecular Characteristics of the Copolymers

sample	octadecyl[a] (%)	M_n[b] (g/mol)	M_h[c] (g/mol)	M_h[d] (g/mol)	DP_{th}[e]
PMLG	0	8 700	8 900	34 300	60
MS10	10	10 000	10 400[f]	4 000[f]	60
MS18	18	11 000	11 600[f]	44 600[f]	60
MS30	30.5	13 000	13 400[f]	51 700[f]	60
MS47	47	15 000	15 900[f]	61 200[f]	60
PSLG	100	23 000	23 700[f]	91 500[f]	60

[a] Percentage of the monomeric unit in the polymer (%). [b] Number average molecular weight (theoretical). [c] Viscosity average molecular weight (from eq 2). [d] Viscosity average molecular weight (from eq 1). [e] Degree of polymerization given by the monomer-initiator ratio. [f] These values were obtained using eq 3.

γ-Octadecyl-L-glutamic acid-*N*-carboxy-anhydride (IV). The desired compound was obtained (6.35 g/74.71% yield) as a white crystalline powder. ^1H NMR (300 MHz, $CDCl_3$): δ = 6.49 (bs, 1H, NH), 4.37 (t, 1H), 4.07 (t, 2H), 2.53 (t, 2H), 2.25 (m, 1H), 2.12 (m, 1H), 1.60 (m, 2H), 1.23 (m, 30 H), 0.86 (t, 3H).

γ-Methyl-L-glutamic acid-*N*-carboxy-anhydride (V). The desired compound was obtained (17.65 g/75.71% yield) as a white crystalline powder. ^1H NMR (300 MHz, $CDCl_3$): δ = 6.60 (bs, 1H, NH), 4.39 (t, 1H), 3.70 (s, 3H), 2.55 (t, 2H), 2.25 (m, 1H), 2.12 (m, 1H).

General Polymerization Procedure. The ring-opening anionic polymerizations were carried out following the standard conditions for NCA polymerizations[19−25] (Scheme 2). The NCA polymerizations were initiated by a primary amine (*n*-hexyl amine) in dry THF. The reactions were stirred at room temperature for 5 days under argon. The random copolymers were obtained by mixing the different NCA monomers in the desired ratio. The polymers were precipitated from methanol and purified by several washings with methanol.

Characterization. The compositions of the copolymers were calculated based on integrations of the ^1H NMR spectra and found to be consistent with the ratio of the monomers. The molecular weight was determined by two different methods. The first method compares the integration of the endgroup signals from the initiator and the polymer backbone resonances in the ^1H NMR spectra. The calculated degree of polymerization (DP) was in agreement with the applied monomer/initiator ratio during polymerization. It should be noted, however, that this method becomes less accurate with increasing DP. Other common characterization methods for polymers, like gel permeation chromatography (GPC) and static light scattering (SLS), had little success due to low solubility, low molecular weights, and tendency of the polymers to aggregate. Viscometry was applied as a second method to determine the molecular weights. Dichloroacetic acid (DCA) (a solvent known to lead to a nonhelical polymer conformation) was used as the eluent to avoid aggregation. Measurements were carried out at 25 °C using an Ubbelohde capillary viscosimeter. Two different Mark−Houwink equations were taken into account calculating M_η[26,27]:

$$[\eta] = (2.78 \times 10^{-5}) M_\eta^{0.87} \quad (1)$$

$$[\eta] = (29 \times 10^{-5}) M_\eta^{0.74} \quad (2)$$

Both equations are valid for DCA at 25 °C but for different polymers. Equation 1 is the well-known relation established by Doty et al.[26] for poly(γ-benzyl-L-glutamate) (PBLG). However, the polymer herein differs with respect to the nature of the side group. Equation 2 was established by Tanaka et al.[27] especially for poly(γ-methyl-L-glutamate) (PMLG). Both methods (eqs 1 and 2) were employed in calculating the molecular weights.

Scheme 1. Synthesis of the NCA

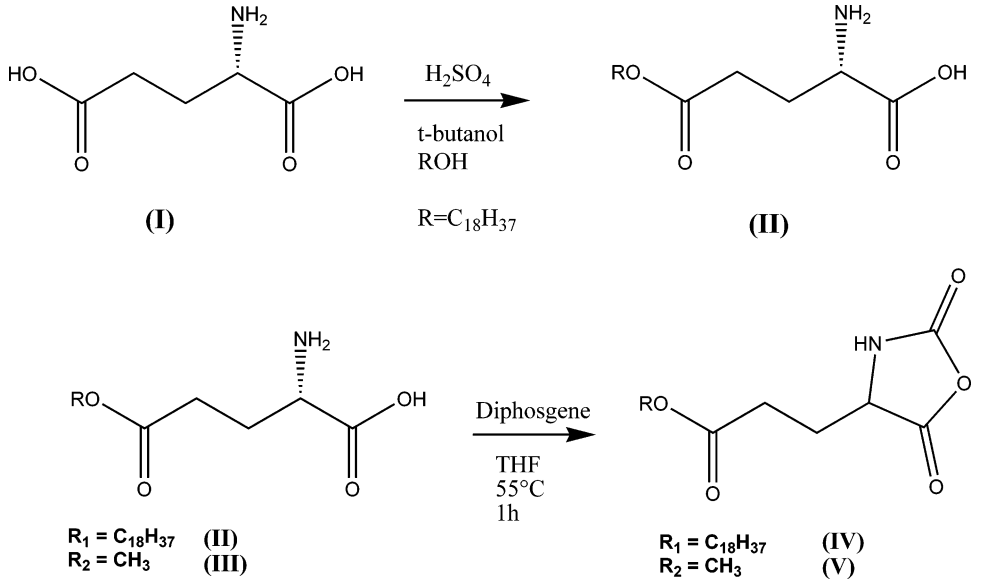

Scheme 2. Ring Opening Anionic Polymerization of the NCAs

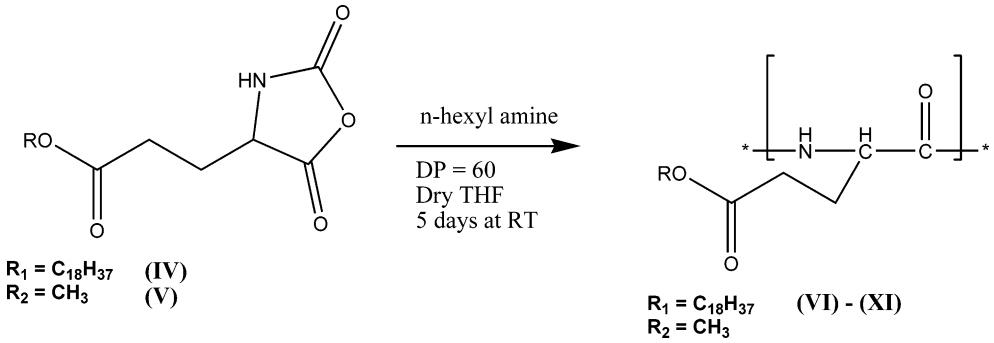

The results, listed in Table 1, exhibit a large disparity for PMLG (polymer **XI**) when applying both sets of Mark−Houwink parameters. In comparing the M_η with the expected values, it is the latter equation that provides the more realistic data. Mark−Houwink parameters for the copolymers as well as for poly(γ-stearyl-L-glutamate) (PSLG) itself in this solvent system do not exist. Therefore the other values of M_η were evaluated according to

$$M_\eta = \left[\left(\frac{M_{\eta,\mathrm{PMLG}} f_{\mathrm{PSLG}}}{M_{\mathrm{R(PMLG)}}}\right) M_{\mathrm{R(PSLG)}}\right] + f_{\mathrm{PMLG}} M_{\eta,\mathrm{PMLG}} \qquad (3)$$

where $M_{\eta,\mathrm{PMLG}}$ is the viscosity average molecular weight of PMLG, $M_{\mathrm{R(PMLG)}}$ is the molecular weight of the repeating unit of PMLG, $M_{\mathrm{R(PSLG)}}$ is the molecular weight of the repeating unit of PSLG, and f are the respective molar fractions in the copolymers.

MALDI-TOF was employed for the homopolypeptides and their copolymers. The polymers were dissolved in a dithranol matrix, and potassium trifluoroacetate was used as a dopant in TFA. This matrix was first reported by Kricheldorf for poly(alanine), poly(sarcosine), and poly(phenylalanine).[28] On the basis of these studies, different mechanisms have been proposed that include a backbiting reaction resulting in chain cyclization, side chain ester group saponification, and cyclization inside the repeating unit giving rise to a stable five ring. All MALDI-TOF spectra from the present polymers (not shown here) support the backbiting reaction. It is estimated that in PSLG the backbiting fraction is about 50% (PMLG exhibits an even higher degree of backbiting) with a high amount of saponificated or cyclized side groups. In addition, NMR revealed the absence of saponification or cyclization in the polymers before dissolution to TFA. Therefore, the pronounced change of structure is due to the highly acidic solvent, which induces the cleavage of the acid labile ester groups. For these reasons MALDI-TOF is not very helpful in characterizing the pristine polymers.

Solid-State NMR. The solid state ^{13}C cross-polarization (CP) NMR experiments on the homopolymers PSLG and PMLG were performed on a Bruker Avance spectrometer with a ^1H Larmor frequency of 700.1 MHz and a ^{13}C frequency of 176.05 MHz. A Bruker double resonance probe, supporting rotors of 2.5 mm outer diameter at a spinning frequency of 30 kHz, was used. At high spinning frequencies, heating effects caused by air friction become significant. The sample temperature was corrected for these frictional heating effects following a known procedure.[29] All other experiments were performed on a Bruker Avance spectrometer with a ^1H Larmor frequency of 500.1 MHz and a ^{13}C frequency of 125.76 MHz, using a standard 2.5 mm Bruker probe at 25 kHz spinning frequency. For all solid-state ^{13}C cross-polarization (CP) magic angle spinning (MAS) NMR experiments, an initial 90° pulse with 2.5 μs length and 2 s recycle delay were used. The duration of the ramped CP pulse was 1 ms, and the TPPM ^1H decoupling scheme[30] was used while acquiring the ^{13}C signal. Transients of 2 k were averaged for the experiments. The spectra were baseline-corrected, and a broadening of 10 Hz was applied. All dipolar recoupling experiments were carried out with equal excitation and reconversion times. The REDOR based recoupled polarization transfer heteronuclear dipolar order rotor encoding (REPT-HDOR)[31,32] was used for $^1H-^{13}C$ double quantum NMR to excite heteronuclear two-spin coherences under recoupling conditions. The analysis of the recorded sideband patterns yielded effective dipole−dipole couplings depending on internuclear distances and molecular dynamics. For the $^1H-^{13}C$ rotor encoded REDOR (REREDOR) spinning sideband patterns,[33] one full rotor period was recorded in the indirect dimension, with the time increment set to 2.0 μs and 25 kHz magic angle spinning frequency.

X-ray Scattering. Wide-angle X-ray scattering (WAXS) measurements were made from macroscopically oriented (extruded) filaments (at $T = 343$ K) with a diameter of 0.7 mm using a pinhole collimation and a two-dimensional detector (Siemens A102647) with 1024 × 1024 pixels. A graphite monochromator was used ($\lambda = 0.154$ nm), and the sample-to-detector distance was 7.2 cm. Measurements were made at selected temperatures: 298, 313, 393, and 433 K by heating.

Dielectric Spectroscopy (DS). The sample cell consisted of two electrodes with 20 mm in diameter, and the sample with a thickness of 50 μm maintained by Teflon spacers. The dielectric measurements were made at different temperatures in the range from 123 to 453 K, at atmospheric pressure, and for frequencies in the range from 10^{-2} to 10^{6} Hz using a Novocontrol BDS system composed of a frequency response analyzer (Solartron Schlumberger FRA 1260) and a broadband dielectric converter. The complex dielectric permittivity $\epsilon^* = \epsilon' - i\epsilon''$, where ϵ' is the real and ϵ'' is the imaginary part, is a function of frequency ω, temperature T, and pressure P, although here only the frequency and temperature dependencies have been investigated.[34] The analysis has been made using the empirical equation of Havriliak and Negami:[35]

$$\frac{\epsilon^*(T,P,\omega) - \epsilon_\infty(T,P)}{\Delta\epsilon(T,P)} = \frac{1}{[1 + (i\omega\tau_{HN}(T,P))\alpha]^\gamma} \tag{4}$$

where $\tau_{HN}(T,P)$ is the characteristic relaxation time in this equation, $\Delta\epsilon(T,P)$ is the relaxation strength of the process under investigation, ϵ_∞ is the dielectric permittivity at the limit of high frequencies, and α, γ ($0 < \alpha, \alpha\gamma \leq 1$) describe, respectively, the symmetrical and asymmetrical broadening of the distribution of relaxation times. The relaxation times at maximum loss (τ_{max}) are presented herein and have been analytically obtained by the Havriliak−Negami equation as follows:

$$\tau_{max} = \tau_{HN}\left[\frac{\sin\left(\frac{\pi\alpha}{2(1+\gamma)}\right)}{\sin\left(\frac{\pi\alpha\gamma}{2(1+\gamma)}\right)}\right]^{-1/\alpha} \tag{5}$$

The linear rise of ϵ'' at lower frequencies is caused by the conductivity ($\epsilon'' = \sigma/(\omega\epsilon_f)$, where σ is the dc-conductivity and ϵ_f is the permittivity of free space) which has been included in the fitting procedure. The measured ϵ'' spectra have been used for the analysis except at high temperatures where the derivative of ϵ' has been employed ($d\epsilon'/d\ln\omega \sim -(2/\pi)\epsilon''$). Since ϵ' is not affected by the conductivity, this method is very useful in fitting relaxation processes which are hidden under the conductivity, provided that the system is free of surface polarization effects. Therefore the latter representation was employed in the analysis of the slower process.

In a second approach we used the electric modulus representation:[34,36]

$$M^* = \frac{1}{\epsilon^*} = M' + iM'' \tag{6}$$

This representation is very sensitive to the presence of slow processes (see below) and to the process due to ionic mobility. The relaxation times corresponding to the M'' maximum are close to the ones from the ϵ'' and are related through $\tau_{M''} = \tau_\epsilon''(1 + \Delta\epsilon/\epsilon_\infty)^{-1/\alpha}$ in the case of a symmetric distribution ($\gamma = 1$).

III. Results and Discussion

Polypeptide Secondary Structure. It is well-known that the ^{13}C chemical shifts are sensitive probes of the peptide local conformation, and thus the ^{13}C cross-polarization-magic angle spinning (CP-MAS) solid-state NMR technique has been widely employed in identifying the predominant polypeptide secondary structures (α-helices and β-sheets).[37,38] The observed differences in chemical shifts of the secondary structures arise from variations of the dihedral angles (Φ and Ψ) depending on the local conformation of individual amino acid residues and is correlated with the type of hydrogen bonding (i.e., intra- or intermolecular). Figure 1 gives the ^{13}C CP-MAS NMR spectra of PSLG (top), PMPG (bottom), and the copolymer MS30 (middle) recorded at 323 K. In the PSLG ^{13}C spectrum, the signals with chemical shifts (δ) at 172.3 and 52.9 ppm arise from the amide C═O and the C_α carbon, respectively, and indicate the formation of β-sheets, whereas the signals at 175.2 and 57.3 ppm reflect α-helical conformations. The peak overlap between the ^{13}C resonances of the amide and ester C═O groups in the 172 ppm region precludes obtaining the ratio of α-helices to β-sheets from this chemical shift. Moreover, using the cross-polarization technique to enhance the low-γ nuclei signal intensity leads to qualitative, rather than quantitative, signal evaluation. Therefore, only the C_α spectral region was used in obtaining the ratio of α-helices to β-sheets, and this ratio for PSLG amounts to 60:40.

The resonances for the pending PSLG side groups are also observed in the region from 14.6 ppm, corresponding to the terminal methyl group, to 33.0 ppm for the dominant CH_2 side group signal. In addition, the OCH_2 group carbon signal appears at 64.5 ppm. The 33.0 ppm methylene peak is indicative of significantly stretched stearyl chains adopting trans conformations, while the approximately 30 ppm shift indicates gauche containing conformers (similar to the noncrystalline regions of polyethylene).[33] Additionally, the predominant trans conformation suggests the presence of abundant crystalline regions in the stearyl side chains with minor amorphous domains. This is in good correlation with the degrees of crystallinity determined from the corresponding heats of fusion for the respective CH_2 side chain moieties in the homo- and copolymers (see below). All aliphatic ^{13}C resonances (with the exception of the CH carbon in the 52−57 ppm region) are sharp with widths at half-height ranging from 140 to 215 Hz. The sharp peaks and the concomitant improved resolution are an indication of high conformational order for the crystalline regions. In the amorphous regions, i.e., the hydrocarbon chain ends, fast side group dynamics lead to averaging of the ^{1}H dipole−dipole couplings at the effective experimental temperature (323 K). The ^{13}C resonances of the methylene moieties in the transitional regions between crystalline and amorphous domains contribute to the broadening of the base of the alkyl peak. At the same time, the inhomogeneous broadening of the C═O and CH carbon peaks (width at half-height from 390 to 560 Hz), due to overlapping spectral frequencies and/or a distribution of conformations, limits the information about the peptide backbone dynamics from the CP-MAS spectrum.

In the ^{13}C CP-MAS spectrum of MS30 (see Figure 1), the dominating CH_2 resonance is at approximately 30 ppm, suggesting disordered chains in gauche conformation. The 33.0 ppm peak, inherent for the low-energy trans-chain conformation, is detected as a very weak shoulder, which separates as an individual resonance only at low temperatures. The different conformation of the SLG hydrocarbon chains in MS30, compared to those in the PSLG homopolymer, is related to the free spatial volume introduced by MLG (abundant) units in the copolymer and occurs for thermodynamic reasons. As previously described,[8] the side chain conformation is related to the backbone organization. Thus, the very weak or absent 33.0 ppm peak implies the formation of rather small pure SLG domains in MS30 with a majority of random MLG/SLG backbone units.

On the other hand, in the ^{13}C CP-MAS solid-state NMR spectrum of PMLG (Figure 1), the traditional probes for the

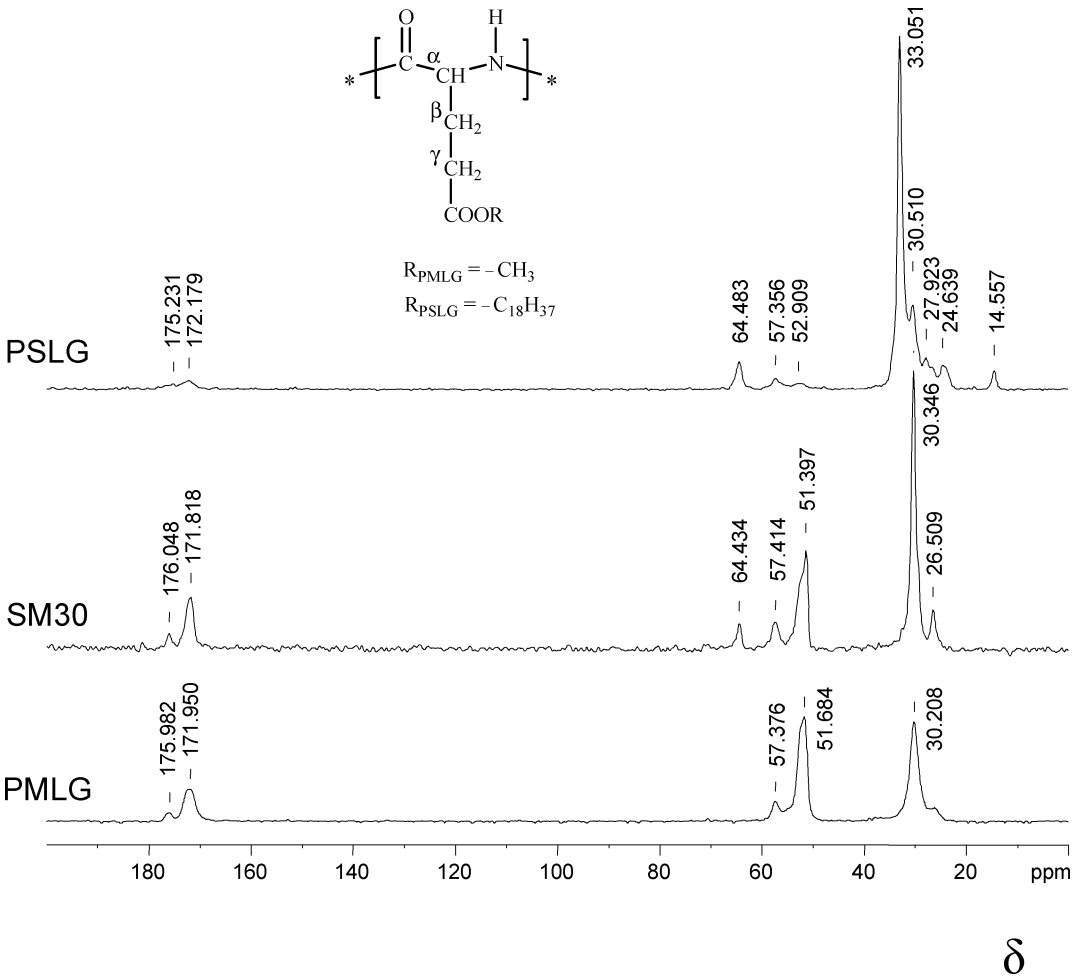

Figure 1. ^{13}C cross-polarization (CP) NMR spectra of PSLG (top), MS30 (middle), and PMLG (bottom) recorded at fast magic angle spinning, 323 K effective sample temperatures, duration of the contact polarization pulse 1 ms, and ^{1}H TPPM decoupling scheme. In PSLG, the α-helix to β-sheet ratio is 60:40, based on the C_α resonances at $\delta \approx 57.3$ and 52.9 ppm, corresponding to α-helices and β-sheets, respectively. In MS30 and PMLG, both α-helices ($\delta \approx 176$ and 57.4) and β-sheets ($\delta \approx 172$ and 51.7) exist but their deconvolution is not possible. The 33 ppm peak, attributed to extended trans conformation of the stearyl side chains, in the ^{13}C CP-MAS spectrum of PSLG is not present in the MS30 spectrum at the same temperature due to the free spatial volume originating from the MLG units.

peptide secondary conformation (CH and C═O carbon resonances) cannot provide unambiguously the ratio of secondary structures due to peak overlap in both the amide C═O (with the ester C═O moiety) and the CH β-sheet (with the OCH_3 group at $\delta \sim 51.6$ ppm) spectral regions. Clearly, α-helices exist in the secondary organization of PMLG as indicated by the ^{13}C signals at 176.0 and 57.4 ppm. The peptide backbone contains also β-sheets, as the signals at 172.0 and 51.7 ppm are significantly stronger as compared to those associated with the α-helical secondary structure. Notice that a pure α-helical conformation would lead to two peaks with comparable intensities in the C_β carbon region at $\delta \sim 30$ ppm,[38] as the β- and γ-CH_2 groups have similar nature and environment and thus cross-polarization efficiency.

We should mention here that the precipitation conditions can influence the peptide secondary structure. For example, a preparation of PSLG with different precipitation conditions (in a shorter time), albeit from the same solvent, resulted in a lower α-helical content (α-helix to β-sheet ratio of 40:60) with consequences on the dynamics (see below). It is the presence of both types of secondary structures in the homopolymers and the proximity of the chemical shifts that makes the deconvolution of the peptide secondary structures in the copolymers a difficult task (independent of the method used). Therefore, in the copolymers we assume the existence of both types of secondary structures.

Thermal and Thermodynamic Properties. Thermal probes are employed to explore the possible side chain crystallization of PSLG in the copolymers as well as the freezing of the copolymer main chain dynamics at the liquid-to-glass temperature. Although the crystallization/melting of SLG in similar copolymers has been investigated in the past,[8,39] the origin of the freezing of the dynamics at T_g for the homopolymers and copolymers remains unclear. The DSC traces of the investigated systems, obtained on heating at 10 K/min, are shown in Figure 2. An endothermic peak is evident with an area that is a function of the PSLG content suggesting the presence of PSLG sequences, at least for the MS18, MS30, and MS47 copolymers. At temperatures below the melting endotherm, a single glass temperature can be identified in the copolymers from the steplike change in the heat flow. The thus obtained T_g values in the copolymers and the (apparent) melting temperatures, T_m', are depicted in Figure 3. In the same figure, the glass temperatures obtained from dielectric spectroscopy (see below) for the copolymers as well as for the homopolymers are included. The copolymer T_g can be described by the Gordon−Taylor equation[40]

$$T_g = (w_1 T_{g_1} + K w_2 T_{g_2})/(w_1 + K w_2) \qquad (7)$$

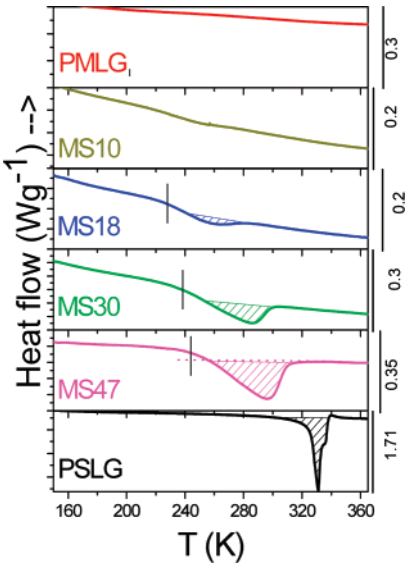

Figure 2. DSC traces obtained during the second heating run (rate 10 K/min), indicating an endothermic peak whose position and width depend on the PSLG content. The copolymer single glass temperature is marked with the vertical lines. The shaded areas were used to obtain the heats of fusion (ΔH) given in Table 2.

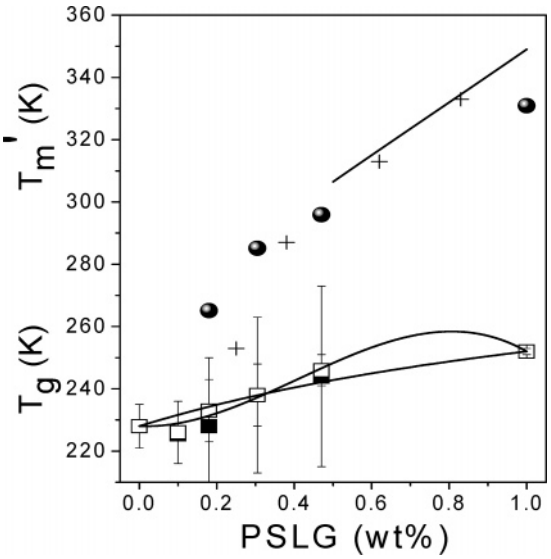

Figure 3. Composition dependence of the single glass temperature T_g from DSC (filled squares) and DS (open squares) and of the apparent melting temperature (filled circles) T_m'. The crosses are the T_m' values from ref 13 whereas the solid line is the linear prediction from ref 38. The solid line to the $T_g(w_{PSLG})$ dependence is the result of the fit to the DS points using the Gordon−Taylor equation, with $K = 1.6 \pm 0.5$. The modified concentration power equation of Schneider et al. (dashed line), provides a better description. The vertical bars give the broadening of the glass temperatures (ΔT_g).

where T_{g_i} and w_i are the glass temperatures and the weight fractions of the homopolymers, respectively, and K is a fitting parameter (assuming volume additivity, $K = \rho_1\Delta\alpha_2/\rho_2\Delta\alpha_1$, where ρ and $\Delta\alpha = \alpha_{melt} - \alpha_{liquid}$ are the density and the increment of the thermal expansion coefficient of the respective components at T_g). A positive deviation from additivity of the glass temperatures is observed, with $K = 1.6 \pm 0.5$. In the case of random copolymers, a second approach by Schneider et al.[41] takes into account the kinetic parameters of the copolymerization reaction which control the sequence distribution (diads and triads) of the copolymers and the contributions of these

Table 2. Thermal and Thermodynamic Parameters of the Copolymers

sample	T_g^{DSC} (K)	T_g^{DS} (K) ($t = 1$ s)	DH (J/g)
PMLG		228	0
MS10	225	226	0
MS18	228	233	~2
MS30	238	238	12
MS47	244	246	21
PSLG		252	69

sequences to the copolymer glass temperature. This results in a modification of the Gordon−Taylor equation in the form

$$(T_g - T_{g_1})/(T_{g_2} - T_{g_1}) = (1 + K_1)w_{2c} - (K_1 + K_2){w_{2c}}^2 + K_2{w_{2c}}^3 \quad (8)$$

where w_{2c} is the corrected weight fraction, $w_{2c} = Kw_2/(w_1 + Kw_2)$, and the new parameters K_1 (-1.2 ± 0.6) and K_2 (-5 ± 1) characterize the contributions of the heterodiads and heterotriads, respectively, to the copolymer T_g. A hint of nonrandom monomer distribution in the copolymers is given by the fact that K_1 is negative ($K_1 = -1.2 \pm 0.6$) which suggests negative deviations from additivity of the copolymer T_g reflecting an increased mobility (due to repulsions within the heterodiads). We will return to this point later with respect to the NMR (Figure 5) and WAXS (Figure 10) studies.

The DS and DSC results on the glass temperatures and the heats of fusion (ΔH) are included in Table 2. The dependence of ΔH on composition is nonlinear. The relatively low enthalpy of melting and the dominance of the extended trans conformations (NMR) point to disordered crystalline regions. Below we will compare these thermodynamic results with site-specific NMR measurements on the same samples that provide a local dynamic order parameter for the main chain and alkyl side groups.

Molecular Dynamics. It may sound paradoxical that methods probing the molecular dynamics can facilitate the self-organization as conventionally probed by, for example, X-ray scattering. In a recent series of publications[5,6,43−45] it was documented that coupling structural techniques with dielectric spectroscopy (DS) in systems containing polypeptides provides both the static and the "dynamic" structure. This is especially the case in polypeptides with an α-helical secondary structure where a macrodipole is formed running from one end of the helix to the other. In such systems, DS has probed the helix persistence length to show that, contrary to expectation and common belief, α-helices are objects of low persistence. The molecular dynamics in the homopolymers and the copolymers can be effectively studied by combining dielectric spectroscopy with site-specific NMR techniques. The former (DS) is well suited in extracting the relevant time scales of the molecular processes. However, a disadvantage of DS is that it cannot provide direct information about the geometry of motion. On the other hand, site-specific NMR techniques can provide the geometry of the motion and when coupled with DS can provide both the geometry and the time scale of motion. We first start with the description of the dynamic NMR experiments and then continue with the DS results.

The $^1H-^{13}C$ REPT-HDOR recoupling solid-state NMR technique performed at fast magic angle spinning has been applied to investigate the molecular dynamics of the PSLG homopolymer and the copolymers MS30 and MS47 at different experimental temperatures. The method is based on recording spinning sideband patterns, from where the effective $^1H-^{13}C$ dipolar coupling constants, D_{CH}, of the different CH_n moieties

Table 3. $^1H-^{13}C$ Dipolar Coupling Constants D_{CH} [kHz] with the Related Local Dynamic Order Parameters for the α-Helical and β-Sheet Backbone CH Segments as Well as the Alkyl Chain Methylene Moieties of the Polymers Investigated[a]

		dipolar coupling constants D [kHz], measured for the CH_n moiety; local dynamic order parameter S		
polymer	T_{eff} (K)	α-helix CH 57 ppm	β-sheet CH 52 ppm	chain CH_2 30 ppm
PSLG	270		21.0	11.8
			~1	0.56
MS47	274	21.0	20.0	9.5
		~1	0.95	0.45
MS30	247	21.0	21.0	11.0[b]; 8.0[c]
		~1	~1	0.52[b]; 0.38[c]
MS30	270	18.5	18.5	9.0
		0.88	0.88	0.43
MS30	363	18.5	19.0	2.5
		0.88	.90	0.12

[a] The $^1H-^{13}C$ dipole−dipole couplings were determined at the respective experimental temperatures analyzing the recorded REPT-HDOR sideband patterns. The experimental conditions were 25 kHz spinning at the magic angle and 80 μs recoupling time in all cases excluding the dipolar coupling of the chain CH_2 groups determined at 363 K using a recoupling time of 320 μs. [b] The $^1H-^{13}C$ dipolar coupling constant (with the respective dynamic local order parameter) determined by analyzing REREDOR1 sideband patterns, recorded at 247 K effective temperature, 25 kHz MAS, 40 μs recoupling time, and initial cross-polarization step for signal enhancement for the methylene groups with a 33.0 ppm chemical shift (trans conformation). [c] The $^1H-^{13}C$ dipolar coupling constant (with the respective dynamic local order parameter) determined for the 30.0 ppm methylene groups (gauche conformation)

in the structure of the copolymers can be extracted and interpreted in terms of local dynamic order parameters, S. The latter are given in the form of the second-order Legendre polynomial[42] and are commonly presented as the ratio of the experimentally determined (effective) dipolar coupling constant of the CH_n group with respect to the coupling of the rigid pair:

$$S = \frac{D_{CH}^{eff}}{D_{CH}^{rigid}} \tag{9}$$

Thus, $S = 1$ stands for totally rigid segments, whereas $S = 0$ results from the complete motional averaging of the dipolar coupling constant of the respective molecular segment due to fast reorientations on the kilohertz time scale. The results of the recoupling $^1H-^{13}C$ REPT-HDOR experiments are summarized in Table 3.

Clearly, the peptide backbone is relatively rigid for MS30 and MS47, as well as for PSLG at about 270 K (Table 3) and at $f \sim 25$ kHz, as determined by the $^1H-^{13}C$ dipolar coupling constants in the range 18.5−21.0 kHz with corresponding local dynamic order parameters being close to 1. This is depicted for the MS30 copolymer at 270 K in Figure 4. The measured $^1H-^{13}C$ dipolar coupling constants for the β-sheet CH pairs compared to those associated with the α-helical conformation in the copolymers MS30, as well as in MS47, are of equal strength. The slight decrease of the backbone local dynamic order parameter for MS30 ($S = 0.88$) compared to $S = 0.95-1.0$ for the MS47 is not significant and in the range of the method error. Surprisingly, a significant overshoot of the first-order sidebands, recorded for the β-sheet CH coupled pair (52 ppm) in MS30 is observed in Figure 4. This is attributed to the reduced $^1H-^{13}C$ dipole−dipole coupling constant of the mobile PMLG methoxy group, which resonates at a similar frequency as the β-sheet CH carbon. As reported,[42] the $^1H-^{13}C$ dipolar coupling constant of a rigid (on microseconds time scale) CH_3 group is scaled by the fast picoseconds rotations of the protons about the internal 3-fold symmetry axis. Additionally, the heteronuclear $^1H-^{13}C$ coupling can be reduced down by rotation or angular fluctuations around the C−O bond axis, which are not excluded at the experimental temperatures. Thus, in the REPT-HDOR sideband pattern, recorded at fast spinning, the OCH_3 moiety is characterized only by first-order sidebands. In the case of MS30, these are superimposed with the sideband pattern recorded at 25 kHz MAS for the rigid peptide backbone, as shown in Figure 4. These results suggest a relatively rigid backbone at the temperature and frequency investigated, where only small-angle backbone fluctuations are allowed.

Considering the alkyl chains, a clear decrease of the local dynamic order parameter from the homopolymer PSLG ($S = 0.56$) to the copolymers ($S = 0.43-0.45$) is observed at 270 K. Obviously, the presence of PMLG with its short side chains in the copolymers leads to higher spatial freedom of the mobile stearyl chains of PSLG and thus to reduced $^1H-^{13}C$ dipolar couplings. In addition, the conformation of the SLG hydrocarbon chains transforms from trans to gauche, leading to amorphous, rather than crystalline side groups, and enhanced chain mobility. A low temperature (247 K) $^1H-^{13}C$ REREDOR solid-state NMR experiment was applied to determine the dipolar couplings of the methylene moieties in both conformations in the copolymer MS30. As expected, the $^1H-^{13}C$ dipole−dipole couplings for the *trans*-methylene groups (approximately 11 kHz) were higher than those measured for the CH_2 groups (approximately 8 kHz) in gauche conformation. Higher temperatures promote increased hydrocarbon methylene moieties mobility. This finding is in agreement with the thermodynamic results that suggested a reduced crystal thickness in the copolymers as compared to bulk PSLG (Table 2). Increasing the experimental temperature from 270 to 363 K does not significantly influence the backbone mobility in MS30, which remains relatively rigid ($S \approx 0.88$). However, the overall chain mobility increases resulting in a pronounced motional averaging of the dipolar couplings and to an improved spectral resolution. Thus, elevated temperatures lead to a splitting of the signal characteristic for the β-sheet conformation as depicted in Figure 5. Clearly, the ^{13}C resonance at about 52.7 ppm is associated with the PSLG β-sheet secondary conformation, whereas the 51.2 ppm signal is attributed to the secondary conformations containing MLG units (see also Figure 1 and the X-ray data below). This signal splitting implies the presence of separated backbone sequences of PMLG and PSLG, in the copolymers with $n \geq 30\%$, which probably occurs for statistic, rather than thermodynamic reasons. This finding suggests some blockiness in the copolymers and will be discussed below with respect to the X-ray results and Figure 11.

Dielectric spectroscopy (DS) is well-suited for studying the molecular dynamics in polypeptides; it has been employed in the past for studying (i) local relaxations below $T_{g'}$,[43] (ii) the origin of the liquid-to-glass transition,[5,6] and (iii) the relaxation of the α-helical secondary structure through the strong dipole of the peptide bond (typical type-A polymer).[44,45] Herein we are mainly concerned with relaxations above T_g and therefore will discuss the α-process associated with the freezing of the dynamics at T_g and the "slower" process associated with the relaxation of the peptide secondary structure. In Figure 6, we show the superposition of the real and imaginary parts of the electric modulus M^*, the dielectric permittivity ϵ^*, as well as of the derivative of the real part of ϵ^* for the PSLG and PMLG homopolymers. The two representations emphasize different features of the same processes. The electric modulus representa-

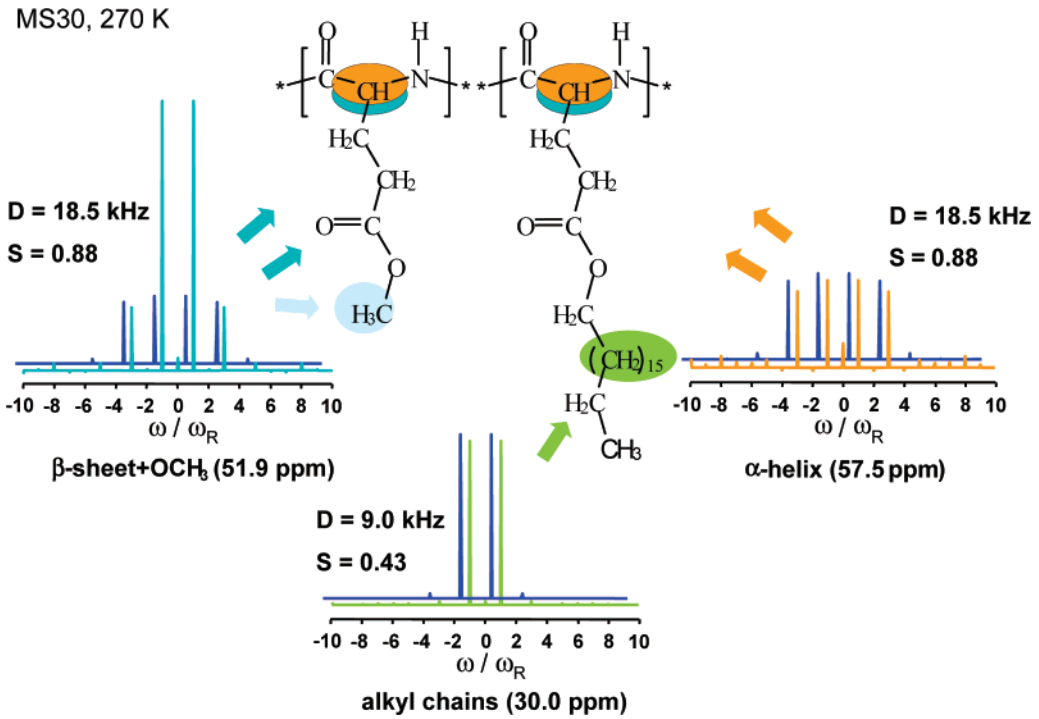

Figure 4. REPT-HDOR sideband patterns recorded at 25 kHz spinning at the magic angle, 80 μs recoupling time, and 270 K effective temperature for the MS30 copolymer; together with the extracted $^{1}H-^{13}C$ dipolar couplings and the related local dynamic order parameters. Overlapping orange and blue colors in the CH backbone region indicate that both α-helical and β-sheet secondary conformations are present in the MS30 backbone. The weak $^{1}H-^{13}C$ dipolar coupling of the PMLG terminal methoxy group (light blue) contributes exclusively to the first-order sideband intensity in the spinning sideband pattern recorded for the β-sheet CH moiety (51.9 ppm).

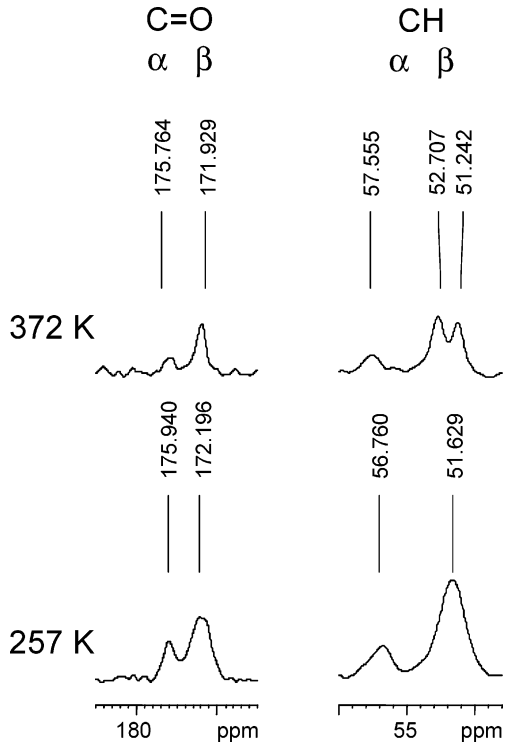

Figure 5. C═O and CH regions of the ^{13}C CP NMR spectra of MS30, recorded at 25 kHz spinning at the magic angle at 363 K (top) and 257 K (bottom). Notice the splitting of the CH β-sheet peak in the high-temperature spectrum.

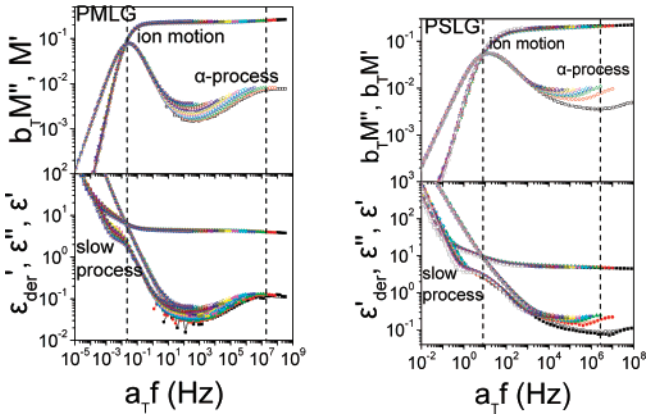

Figure 6. Superposition of the real (filled symbols) and imaginary (open symbols) parts of the electric modulus M^* and of the complex dielectric permittivity ϵ^* for the homopolymers at a reference temperature of 340 K. The superimposed data sets are taken in intervals of 10 or 5 K within the temperature range 240−430 K and 323−413 K for PMLG and PSLG, respectively.

tion provides the α-process at higher frequencies and the ionic mobility, from the crossing of the real and imaginary parts, at lower frequencies/high temperatures. On the other hand, the dielectric permittivity representation provides the α-process as well as a slower process associated with the relaxation of the peptide secondary structure. Notice that the PSLG α-process is hardly seen in the DS spectra because of side group crystallization that broadens and diminishes the dielectric strength of the process (dipoles are located in the vicinity of the crystallizing methylene units). This results in the pronounced failure of the time−temperature superposition (tTs) for PSLG. The tTs fails also for PSLG but for a different reason; the process becomes narrower with increasing temperature. The origin of the α-process in polypeptides has been the focus of our recent attention.[5,6] It reflects the relaxation of amorphous segments at the backbone and at the chain-ends and as such is independent from the peptide secondary structure, the presence of side groups, etc. Thus the liquid-to-glass transition is an inherent feature of the peptide dynamics associated with breaking of hydrogen bonds at certain points called “defects”.

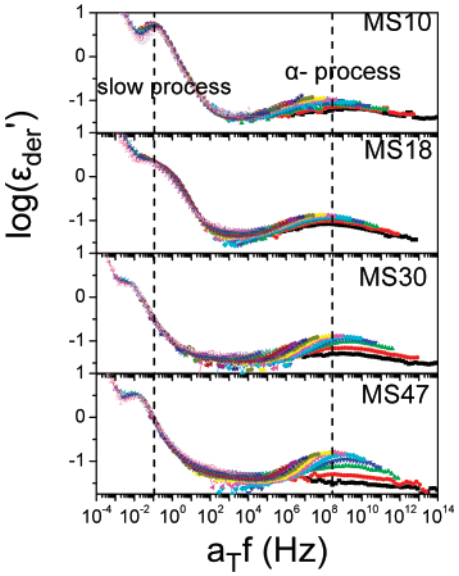

Figure 7. Calculated conductivity-free dielectric loss spectra for the copolymers. The reference temperature is 343 K and the temperature range 240−413 K in 10 K increments. The dashed lines give the positions of the slow and the α-process maxima. Notice the breakdown of time−temperature superposition in the vicinity of the α-process due to PSLG crystallization and the slow down of the slow process with increasing PSLG content.

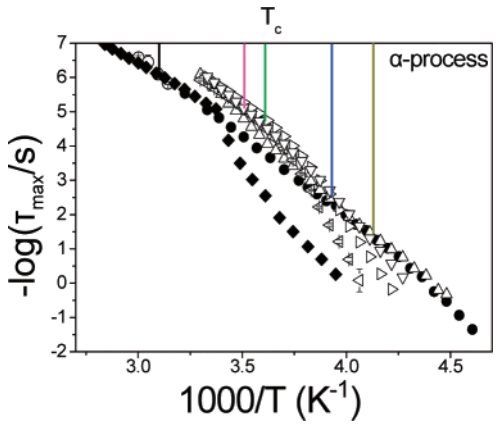

Figure 8. Arrhenius plot of the segmental (α-) process obtained on cooling: PMLG (filled circles), MS10 (up triangles), MS18 (down triangles), MS30 (right triangles), MS47 (left triangles), PSLG (open circles), pODMA (diamond).[45] The vertical lines correspond to the PSLG crystallization temperature (T_c) obtained from DSC.

In Figure 7, we compare the copolymer spectra obtained from the derivative of the dielectric permittivity at the same reference temperature (T_{ref} = 343 K). There is a single α-process in the copolymers and the effect of stearyl crystallization can clearly be seen in the spectral broadening upon lowering the temperature for MS47 and MS30. On the other hand, stearyl in MS10 does not crystallize (Figure 2) and the origin of the tTs failure is the narrowing of the distribution of relaxation with increasing temperature. Notice that the slower process associated with the relaxation of α-helical structures becomes slower with increasing stearyl content. We will return to this point later with respect to Figure 9.

The relaxation times associated with the segmental (α-) process of the homopolymers along with the respective copolymers are shown in the usual Arrhenius representation in Figure 8. The relaxation times display the usual non-Arrhenius T-dependence that conforms to the Vogel−Fulcher−Tammann (VFT) equation

$$\tau_{max} = \tau_0 \exp\frac{D_T T_0}{T - T_0} \qquad (10)$$

where D_T is a dimensionless parameter and T_0 is the "ideal" glass temperature. The PSLG crystallization temperatures, as obtained from DSC, are also indicated in the figure. As discussed earlier with respect to Figure 6, the PSLG α-process can better be studied in the melt state. For comparison, we include in the figure the α-process relaxation times of poly(*n*-octadecyl methacrylate) (pODMA)[46] with a similar side group as PSLG. In the former (pODMA), the α-process dynamics slow down upon side chain crystallization and at these temperatures the process reflects the dynamics of the restricted amorphous phase (RAP). As expected, the segmental dynamics of PSLG and pODMA are similar in the range where experimental points are available. Furthermore, the PSLG $\tau_\alpha(T)$ exhibit a dependence known from "strong" liquids with only a slight curvature in this representation. With respect to the copolymers, we notice that the single α-process is sensitive to the stearyl content. For the amorphous MS10, the dynamics are nearly indistinguishable from PMLG, but starting with MS18, the α-process shows a systematic change with increasing stearyl content. Thus the main effect of the crystallizable PSLG units on the copolymer dynamics is to slow down the α-process and to increase the effective T_g of the RAP (Figure 2). In addition, the $\tau(T)$ dependence in the copolymers is distinctly different from the PMLG homopolymer suggesting an increasing fragility with increasing stearyl content. The steepness index[47] used as a measure of fragility, $m(=\mathrm{d}(\log\tau)/\mathrm{d}(T_g/T))_{T=T_g}$, assumes values of 23, 21, 32, 37, and 53 for PSLG, MS10, MS18, MS30, and MS47, respectively, revealing that side group crystallization makes the RAP relaxation more prone to temperature variations near T_g.

The slower DS process (Figures 6 and 7) associates with the relaxation of α-helical segments, and an analysis of the dielectric strength ($\Delta\epsilon$) of this process allows an estimation of the helix persistence length in the homopolymers and the copolymers. The results for the normalized effective dipole moments are shown in Figure 7. In the calculation we have used the Buckingham equation (modified by Applequist and Mahr) suitable for rigid-rod molecules[48] from where the $\Delta\epsilon$ is given from

$$\frac{Nfg\mu^2}{3\epsilon_0 k_B T} = \frac{(2\epsilon_s + 1)(\epsilon_s - n^2)}{2\epsilon_s + n^2} - \frac{(2\epsilon_\infty + 1)(\epsilon_\infty - n^2)}{2\epsilon_\infty + n^2} \qquad (11)$$

where N is the number density of dipoles (in the calculation we have used for the mass density 1.31 and 1.05 g/cm^3 for PMLG[49] and PSLG,[10] respectively), μ is the dipole moment, f and g are factors related to the geometry of the molecule ($f \rightarrow {}^2/_3$ and $g \rightarrow 1$ for an infinitely long rod), ϵ_s and ϵ_∞ are the unrelaxed and relaxed components of the permittivity for the process under investigation, and n is the refractive index. The effective dipole moment, μ_{eff} $(=g^*\mu^2)^{1/2}$, where g^* is the Kirkwood−Fröhlich pair correlation factor between neighboring dipoles, are plotted in the figure. The thus obtained values, normalized to the corresponding values for the α-process, are compared with the corresponding moments assuming a perfectly α-helical PMLG polypeptide (dashed line) with a degree of polymerization of 60. (The dipole moment per monomer was calculated with ArgusLab and found to be 3.3 D/monomer for

PMLG and 3.7 D/monomer for PSLG). The measured effective dipole moments for PMLG and the copolymers are consistently smaller than the ones corresponding to a perfect α-helix suggesting that helices are far from ideal. Consequently, helices are considered to be broken at several places called "defects" along the backbone.[36,44,45] As we have pointed out recently, it is the relaxation of these "defects" along the polymer backbone that give rise to the slower DS process. A typical helix persistence length of the order of 2 nm was found in poly(γ-benzyl-L-glutamates).[36] These results reveal that the PSLG, PMLG, and the copolymer backbones cannot be considered as perfectly rigid and this dynamic feature has direct consequences on the self-assembly. This result does not contradict with the NMR experiment that suggested a high local dynamic order parameter ($S \sim 0.88$) for the backbone since small amplitude fluctuations are still possible in the peptide backbone.

Last, the effect of the precipitation conditions is not only to change the ratio of α-helices to β-sheets but also to change the dynamics of the slower processes. For example, in the new synthesis of PSLG with the lower α-helical content, the slower process associated with the relaxation of the secondary structure speeds up (not shown here).

Self-Assembly. Knowledge of the type of peptide secondary structure (NMR) and of the persistence of α-helices (DS) coupled with diffraction experiments from oriented fibers can provide a realistic picture of the self-assembly in the copolymers. Figure 10 compares the two-dimensional X-ray diffraction images and the equatorial intensities of the homopolymers and of the copolymers. The diffraction pattern from the PSLG fibers contains a series of intense, albeit broad, equatorial reflections at wavevectors 1.73, 3.52, and ~5.7 nm^{-1} with indices of *h*00 (i.e., 100, 200, and 300) and a broad wide-angle meridional reflection at 14.3 nm^{-1}. These reflections suggest a layered structure for PSLG at room temperature, composed from backbones aligned along the fiber axis in layers with the side groups emanating from the backbones with their axes perpendicular to the layers forming a neighboring "*n*-alkane" layer. The average interlayer distance is about 3.6 nm (first strong equatorial reflections) with approximately seven methylene units incorporated within the paraffin layer. The latter shows the characteristic distance of 0.44 nm that corresponds to the usual triclinic unit cell found in crystals of *n*-alkanes.[50] In an earlier study, the distance between neighboring backbones within each backbone layer was estimated as 1.23 nm from the known density and by assuming a repeat length of 2.7 nm corresponding to a perfect PSLG α-helix. Clearly, such a length cannot be extracted here for two reasons: first, PSLG consists of both α-helices and β-sheets (Figure 1) and second, α-helices are defected (Figure 9).

The corresponding profile obtained from the extruded PMLG fiber contains a broad equatorial reflection at a higher wavevector (at 5.55 nm^{-1} with a corresponding spacing of ~1.13 nm), signifying aligned backbones along the fiber axis and with the shorter side group giving rise to the shorter backbone-to-backbone correlations. We mention here parenthetically, that films prepared from chloroform solutions exhibited a highly crystalline structure consisting of α-helices packed in a hexagonal array with a unit-cell dimension of 1.195 nm.[49]

The profiles in the copolymers contain both equatorial peaks (Figure 10) revealing the presence of both PSLG- and PMLG-type interchain correlations. This is depicted in a schematic way in Figure 11a. In Figure 11b, the composition dependence of the equatorial reflections is shown. From the two types of correlations, it is the shorter (PMLG) interchain correlations

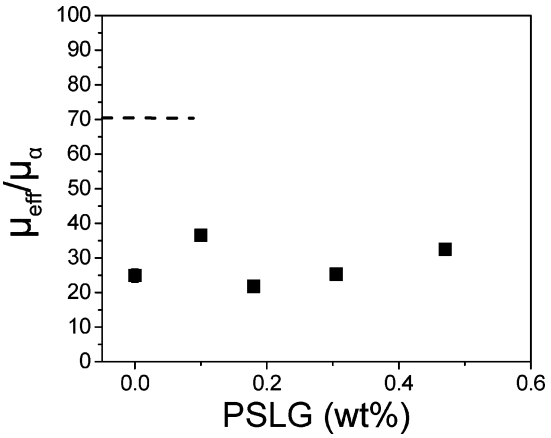

Figure 9. Normalized effective dipole moment of PMLG and the copolymers obtained from the intensity of the slower DS process. The lines indicate the ideal α-helix dipole moment for pure PMLG for a degree of polymerization of 60 and α-helical content of 50% ($\mu_{\alpha PMLG} = 1.41$ D).

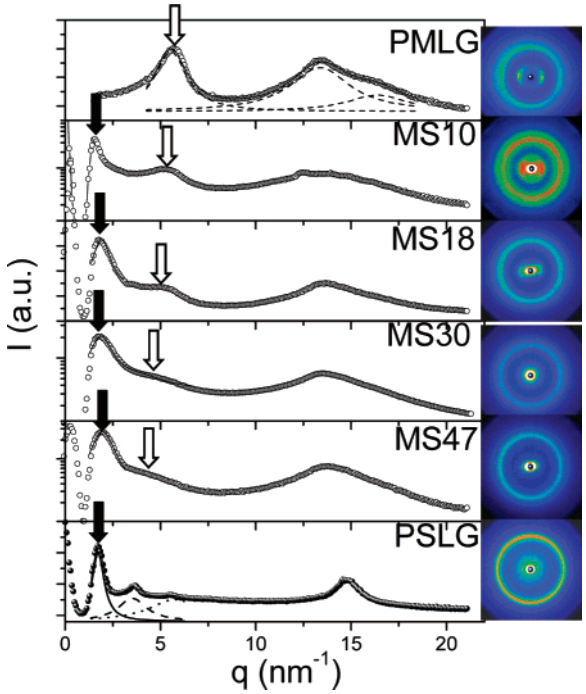

Figure 10. Equatorial WAXS intensity distributions of the homopolymers and the copolymers obtained from oriented fibers at 298 K (left), along with the corresponding 2D images (right). Fiber orientation is along the vertical direction. Notice the presence of two equatorial reflections in the copolymer images. Solid and open arrows give the positions of peaks with correlations between the SLG and random MLG/SLG sequences, respectively (see text). Note that both types of (equatorial) correlations are present in the copolymers.

that seem to be more affected by increasing the PSLG content in the copolymers. This suggests the presence of random MLG/SLG sequences and of more distant SLG sequences. A realistic picture of the self-assembly in the copolymers is given in Figure 11c. Despite being a schematic, the figure contains the main experimental results from the structural (NMR, WAXS) and dynamic (DS, ^{13}C CP NMR) investigations. Extruded polymer chains are oriented along the fiber axis (giving rise to the WAXS equatorial reflections) and have a bottleneck structure with amorphous MLG/SLG units at closer packing (forming the neck) and more distant SLG units (forming the bottle). Similar secondary structures are assumed in the copolymers as in the homopolymers (i.e., a mixture of α-helices and β-sheets) with α-helical structures that are broken at various places (DS).

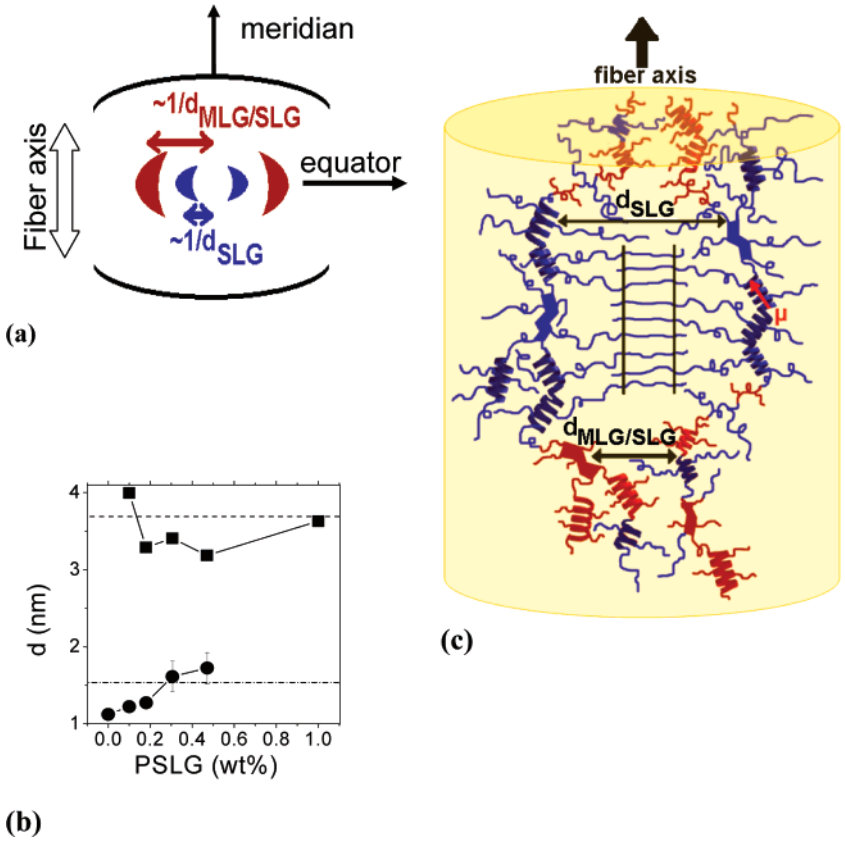

Figure 11. (a) Highly schematic wide-angle X-ray scattering 2D pattern displaying SLG and SLG/MLG intermolecular correlations. (b) Composition dependence of the domain spacing for the different copolymers at $T = 298$ K. Two different spacings are simultaneously present in the copolymers, arising from the longer (SLG, ■) and shorter (MLG/SLG, ●) backbone-to-backbone correlations. (c) Schematic illustration of a 3D arrangement within an oriented copolymer fiber. The experimentally detected characteristic distances correspond to intermolecular SLG (d_{SLG}) and MLG/SLG ($d_{MLG/SLG}$) correlations.

Crystallization takes place only when several stearyl units exist along the copolymer backbone, suggesting the presence of a nonrandom monomer distribution (^{13}C CP NMR).

The model shown in Figure 11c bears only few similarities and has large differences from the three "phase" model suggested in ref 13. The similarities are in the presence of amorphous and crystalline stearyl groups. The main differences are in (i) the presence of both types of secondary structures and the broken α-helical backbones (DS) and (ii) the blockiness giving rise to the bottleneck structure (WAXS).

IV. Conclusions

The main conclusion of this work is that the details of the self-organization in a class of model nanocomposites made from rods embedded into a matrix of flexible side groups requires both structural and dynamic probes. A systematic investigation of the self-assembly and the associated dynamics in a series of poly(γ-methyl-L-glutamate-*co*-γ-stearyl-L-glutamate) was made by combining structural (WAXS, NMR), thermal (DSC), and dynamic probes (DS, site specific NMR) revealing a more complex self-organization than previously thought. The main conclusions are summarized below.

With respect to the structure, (i) the secondary structure of the homopolymers and the copolymers is composed of both α-helices and β-sheets whose ratio depends on the PSLG content and method of precipitation. (ii) Extruded fibers have polymer chains composed of α-helices/β-sheets oriented along the fiber axis with a bottleneck structure with amorphous MLG/SLG units forming the neck and more distant SLG units forming the bottle. (iii) Stearyl crystallization takes place in the copolymers with $w_{PSLG} \geq 18\%$. The relatively low enthalpy of melting (DSC) and the dominance of the extended trans conformations (NMR) point to disordered crystalline regions. The alkyl chain crystallization is reflected in the local dynamic order parameter obtained from NMR with respective values of 0.56 and ~0.44 for PSLG and the copolymers. The crystal thickness depends on the SLG content and is directly related with the SLG chains conformation (see above); decreasing the SLG content in the copolymers makes the crystal thinner as revealed by the nonlinear reduction in the apparent melting temperatures.

With respect to the dynamics, (i) site-specific solid-state NMR techniques identified a relatively rigid backbone ($S \sim 0.88$) in PSLG and in the copolymers that permits only small-angle backbone fluctuations. (ii) Dielectric spectroscopy revealed a "fast" local process in the glassy state and two processes at higher temperatures both with a strong $\tau(T)$ dependence. Although our results for the "fast" process were in agreement with earlier studies, our interpretation of the two VFT processes differs. The first VFT process is associated with the usual liquid-to-glass transition suggesting the presence of amorphous segments in the homopolymers and the copolymers. The single segmental process as well as its $\tau(T)$ is controlled by the SLG content. Furthermore, increasing the SLG content induces a strong-to-fragile behavior as revealed from the systematic dependence of the steepness index. The origin of the "fast" process is small-amplitude motions of the backbone and at the chain-ends as revealed by solid-state NMR. The "slower" DS process with a VFT temperature dependence is associated with the relaxation of the peptide secondary (α-helical) structure.

Nevertheless, in contrast to earlier studies, α-helices are objects of low persistence.

Acknowledgment. The financial support by the Greek Secretariat for Research and Technology (Grants PENED2003, 03ED856) and by the Greek Ministry of Education (Pythagoras I) and the Deutsche Forschungsgemeinschaft (Grant SFB 625) are greatly appreciated. We are indebted to M. Bach, A. Best, and Ch. Herrmann (Max-Planck-Institut für Poymerforschung) and to G. Tsoumanis (University of Ioannina) for technical support.

References and Notes

(1) Wegner, G. *Macromol. Chem. Phys.* **2003**, *204*, 347.
(2) Floudas, G. *Prog. Polym. Sci.* **2004**, *29*, 1143.
(3) Mierzwa, M.; Floudas, G.; Neidhöfer, M.; Graf, R.; Spiess, H. W.; Meyer, W. H.; Wegner, G. *J. Chem. Phys.* **2002**, *117*, 6289.
(4) Gitsas, A.; Floudas, G.; Wegner, G. *Phys. Rev. E.* **2004**, *69*, 41802.
(5) Papadopoulos, P.; Floudas, G.; Schnell, I.; Klok, H.-A.; Aliferis, T.; Iatrou, H.; Hadjichristidis, N. *J. Chem. Phys.* **2005**, *122*, 224906.
(6) Papadopoulos, P.; Floudas, G.; Klok, H.-A.; Schnell, I.; Pakula, T. *Biomacromolecules* **2004**, *5*, 81.
(7) Ballauff, M. *Angew. Chem., Int. Ed.* **1989**, *101*, 261.
(8) Clauss, J.; Schmodt-Rohr, K.; Adam, A.; Boeffel, C.; Spiess, H. W. *Macromolecules* **1992**, *25*, 5208.
(9) Adam, A.; Spiess, H. W. *Makromol. Chem. Rapid Commun.* **1990**, *11*, 249.
(10) Watanabe, J.; Ono, H.; Uematsu, I.; Abe, A. *Macromolecules* **1985**, *18*, 2141.
(11) Romero Colomer, F. J.; Gómez Ribelles, J. L.; Lloveras Maciá, J.; Muñoz Guerra, S. *Polymer* **1991**, *32*, 1642.
(12) Romero Colomer, F. J.; Gómez Ribelles, J. L.; Barrales-Rienda, J. M. *Macromolecules* **1994**, *27*, 5004.
(13) Yamaguchi, M.; Tsutsumi, A. *Polym. J.* **1990**, *22*, 781.
(14) Schmidt, A.; Lehmann, S.; Georgelin, M.; Katana, G.; Mathauer, K.; Kremer, F.; Schmidt-Rohr, K.; Boeffel, C.; Wegner, G.; Knoll, W. *Macromolecules* **1995**, *28*, 5487.
(15) Schmidt, A.; Mathauer, K.; Reiter, G.; Foster, M. D.; Stamm, M.; Wegner, G.; Knoll, W. *Langmuir* **1994**, *10*, 3820.
(16) Spiess, H. W. *J. Polym. Sci., Part A: Polym. Chem.* **2004**, 42, 5031
(17) Wassermann, D.; Garber, J. D.; Meigs, F. M. U.S. Patent 3,285,953, 1966.
(18) Katakai, R.; Iizuka, Y. *J. Org. Chem.* **1985**, *50*, 715.
(19) Poche, D. S.; Moore, M. J.; Bowles, J. L. *Synth. Commun.* **1999**, *29*, 843.
(20) Daly, W. H.; Poche, D. S. *Tetrahedron Lett.* **1988**, *29*, 5859.
(21) Poche, D. S.; Daly, W. H.; Russo, P. S. *Macromolecules* **1995**, *28*, 6745.
(22) Daly, W. H.; Poche, D. S.; Negulescu, I. I. *Prog. Polym. Sci.* **1994**, *19*, 79.
(23) Block, H. *Poly(γ-benzyl-L-glutamate) and Other Glutamic Acid Containing Polymers*, Vol. 9, Gordon and Breach: New York, 1983.
(24) Blout, E. R.; Karlson, R. H.; Doty, P.; Hargitay, B. *J. Am. Chem. Soc.* **1954**, *76*, 4492.
(25) Doty, P.; Lundberg, R. D. *J. Am. Chem. Soc.* **1957**, *79*, 2338.
(26) Doty, P.; Bradbury, J. H.; Holtzer, A. M. *J. Am. Chem. Soc.* **1956**, *78*, 947.
(27) Tanaka, S.; Akio, N. *Bull. Inst. Chem. Res., Kyoto Univ.* **1976**, *54*, 229.
(28) Kricheldorf, H. R.; Lossow, C.; Schwarz, G. *Macromolecules* **2005**, *38*, 5513.
(29) Langer, B.; Schell, I.; Spiess, H. W.; Grimmer, A.-R., *J. Magn. Reson.* **1999**, *138*, 182.
(30) Metz, G.; Wu, X.; Smith, S. O. *J. Magn. Reson.* **1994**, *110*, 219.
(31) Saalwächter, K.; Graf, R.; Spiess, H. W. *J. Magn. Reson.* **1999**, *140*, 471.
(32) Saalwächter, K.; Graf, R.; Spiess, H. W. *J. Magn. Reson.* **2001**, *148*, 398.
(33) Saalwächter, K.; Schnell, I. *Solid State Nucl. Magn. Reson.* **2002**, *22*, 154.
(34) Kremer, F., Schönhals, A., Eds. *Broadband Dielectric Spectroscopy*; Springer: Berlin, Germany, 2002.
(35) Havriliak, S.; Negami, S. *Polymer* **1967**, *8*, 161.
(36) Papadopoulos, P.; Floudas, G. *Dielectr. Newsl.* **2005**, Issue Nov.
(37) Kricheldorf, H. R.; Müller, D. *Macromolecules* **1983**, *16*, 615.
(38) Shoji, A.; Ozaki, T.; Saito, H.; Tabeta, R.; Ando, I. *Macromolecules* **1984**, *17*, 1472.
(39) (a) Tsujita, Y.; Ojika, R.; Tsuzuki, K.; Takizawa, A.; Kinoshita, T. *J. Polym. Sci., Part A: Polym. Chem.* **1987**, *25*, 1041. (b) Tsujita, Y.; Ojika, R.; Takizawa, A.; Kinoshita, T. *J. Polym. Sci., Part A: Polym. Chem.* **1987**, *25*, 1041.
(40) Gordon, M.; Taylor, J. S. *J. Appl. Chem. USSR* **1952**, *2*, 493.
(41) Schneider, H. A.; Rieger, J.; Penzel, E. *Polymer* **1997**, *38*, 1323.
(42) Schmidt-Rohr, K.; Spiess, H.W. *Multidimensional Solid State NMR and Polymers*; Academic Press: New York, 1994.
(43) Mondeshki, M.; Mihov, G.; Graf, R.; Spiess, H. W.; Müllen, K.; Papadopoulos, P.; Gitsas, A.; Floudas, G. *Macromolecules* **2006**, *39*, 9605.
(44) Papadopoulos, P.; Floudas, G.; Schnell, I.; Aliferis, T.; Iatrou, H.; Hadjichristidis, N. *Biomacromolecules* **2005**, *6*, 2352.
(45) Papadopoulos, P.; Floudas, G.; Schnell, I.; Lieberwirth, I.; Nguyen, T. Q.; Klok, H.-A. *Biomacromolecules* **2006**, *7*, 618.
(46) Mierzwa, M.; Floudas, G.; Štěpánek, P.; Wegner, G. *Phys. Rev. B.* **2000**, *62*, 14012.
(47) Bohmer, R.; Ngai, K. L.; Angell, C. A.; Plazek, D. J. *J. Chem. Phys.* **1993**, *99*, 4201.
(48) Buckingham, A. D. *Aust. J. Chem.* **1953**, *6*, 323.
(49) Sasaki, S.; Uematsu, I. *J. Polym. Sci.* **1985**, *23*, 263.
(50) Turner-Jones, A. *J. Polym. Sci.* **1962**, *62*, S53.

MA070792I